arXiv:cond-mat/0209055v1 [cond-mat.mtrl-sci] 3 Sep 2002

Defect correlations, metal-insulator transition, and magnetic order in ferromagnetic semiconductors

Carsten Timm and Felix von Oppen
Freie Universität Berlin, Arnimallee 14, D-14195 Berlin, Germany

Abstract. Diluted ferromagnetic III-V semiconductors typically show a high degree of compensation. Compensation is connected to the presence of comparable densities of charged defects of either sign. This naturally leads to the development of strong correlations between defect positions during growth and annealing. We show that these correlations are required to understand the experimentally observed transport and magnetic properties as well as the persistence of the energy gap upon doping with magnetic ions.

1. Introduction

Diluted ferromagnetic III-V semiconductors are promising materials for applications as well as interesting from the physics point of view. They might allow the incorporation of ferromagnetic elements into semiconductor devices, and thus the integration of data processing and magnetic storage on a single chip. It is important to understand the interplay between transport properties, magnetic ordering, and the defect configuration, which is determined by the growth conditions. We show that correlated positions of defects are required for a description consistent with experiments [1].

To be specific, we consider GaAs doped with manganese, but the results should apply for most III-V compounds. The physics relies on the dual role played by the Mn impurities: They carry a local spin due to the half-filled *d*-shell and dope the system with holes, which mediate a ferromagnetic indirect exchange interaction between the spins. A crucial feature of these materials is their high degree of compensation, which is presumably due to antisite defects (As substituted for Ga). The accordingly small density of holes leads to weak electronic screening of the Coulomb interaction between charged defects and between defects and holes. This role of compensation has not been taken into account previously. Due to the strong Coulomb interactions a random distribution of defects on the cation sublattice is very costly in energy. Therefore, defect diffusion [2] leads to a rearrangement of defects in such a way that the Coulomb energy is reduced. We study this rearrangement with the help of Monte Carlo (MC) simulations and find that strong correlations of defect positions develop. The resulting disorder potential acting on the valence-band holes is strongly reduced and most of its correlations fall off on the scale of the minimum defect separation. We show that this effect has tremendous consequences for transport properties, the integrity of the energy gap, and the temperature-dependent magnetisation. In fact, a description in agreement with experiments *requires* the defects to be strongly correlated.

2. Correlated defects

In this section, we study how diffusion of defects, *i.e.*, Mn impurities and antisites, changes the defect configuration and the disorder potential. This is motivated by experiments [2] that

show that defect diffusion is rather pronounced at typical growth and annealing temperatures of the order of 250°C. We start from a random distribution of Mn impuritites and antisites (As) on the cation sublattice, where the density of antisites is determined by charge neutrality from the observed [3] hole concentrations at given Mn doping levels. The Hamiltonian reads

$$H = \frac{1}{2} \sum_{i,j} \frac{q_i q_j}{\varepsilon r_{ij}} e^{-r_{ij}/r_{\rm scr}}, \tag{1}$$

where q_i are the defect charges and r_{ij} is their separation. Relative to the cation sublattice, Mn impurities carry charge $q = -1$ whereas antisites carry $q = +2$. The screening length $r_{\rm scr}$ is obtained from nonlinear screening theory [4]. It is much larger than the nearest-neighbor separation on the cation sublattice so that it hardly affects the small-scale defect correlations relevant here. We perform MC simulations for the Hamiltonian H [1] employing the Metropolis algorithm at the temperature 250°C for systems of $20 \times 20 \times 20$ conventional cubic unit cells with periodic boundary conditions, unless stated otherwise. To roughly model the dynamics, we only use local MC moves, *i.e.*, exchanges of nearest-neighbor defect and/or host atoms. A more realistic modelling of the dynamics involving interstitials and vacancies lies beyond the scope of this work. The resulting configurations are quenched at low temperatures [5].

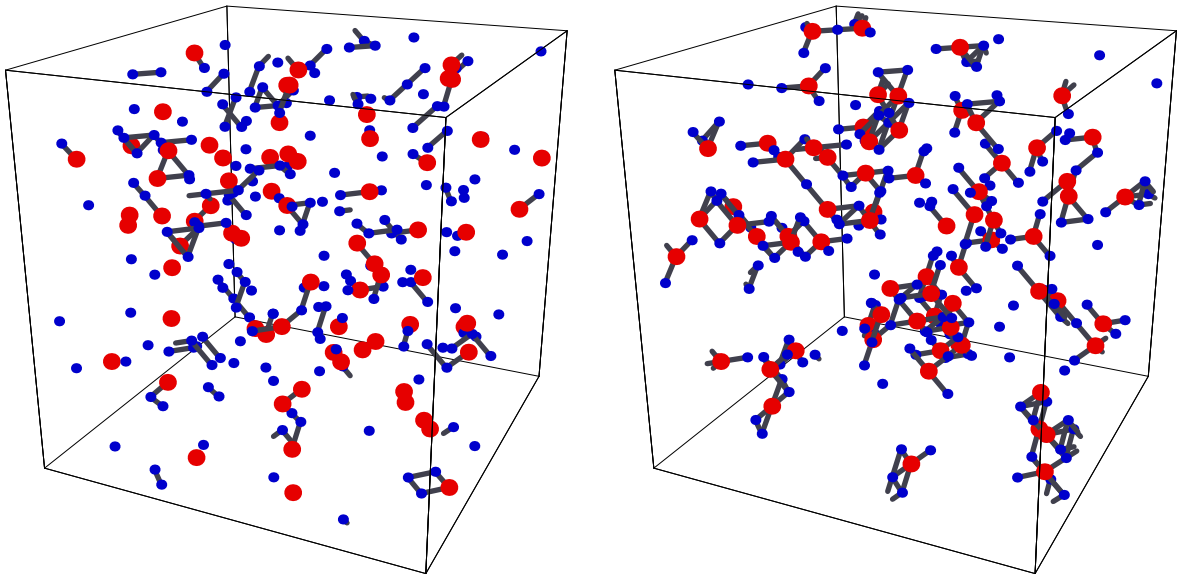


Figure 1. Left: Random configuration of defects on a $10 \times 10 \times 10$ lattice for Mn concentration $x = 0.05$ and $p = 0.3$ holes per Mn. The host lattice is not shown. Small blue circles denote Mn impurities, whereas large red ones are As antisites. When two defects sit on nearest-neighbor sites, they are connected by a solid line. Right: Equilibrated configuration of defects. It is obvious that the defect positions are now strongly correlated.

Figure 1 (left) shows a random configuration of defects for a Mn concentration of $x = 0.05$ and $p = 0.3$ holes per Mn, which determines the concentration of antisites (0.0175). This should be compared to the right part of Fig. 1, which shows an equilibrated configuration of the same number of defects. It is obvious that the defects have formed small clusters, where typically an antisites (charge $+2$) is surrounded by several Mn impurities (charge -1). It is clear that this clustering leads to a strongly reduced impurity potential, since the antisite charges are very effectively screened.

More quantitative information can be obtained from the potential correlation function

$$D(r) \equiv \langle V(\mathbf{r}) V(\mathbf{r}') \rangle_{|\mathbf{r}-\mathbf{r}'|=r} - \langle V \rangle^2. \tag{2}$$

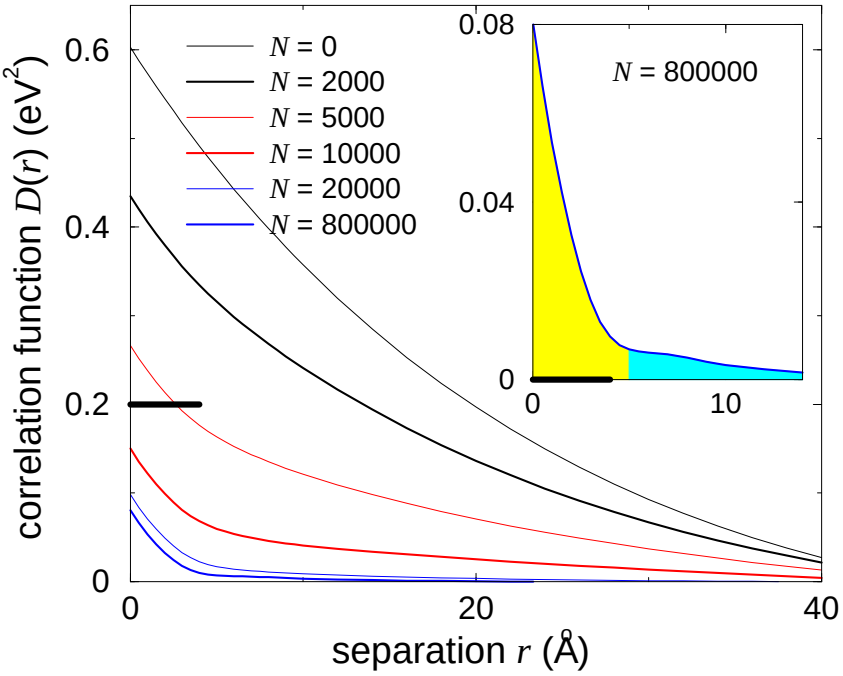


Figure 2. Potential correlation function $D(r)$ for Mn concentration $x = 0.05$ and $p = 0.3$ holes per Mn, plotted for various numbers of MC steps. The heavy solid bar denotes the nearest-neighbor separation on the cation sublattice. The inset shows the initial rapid decrease of $D(r)$ for the equilibrated case, see text.

Obviously, $\Delta V \equiv \sqrt{D(0)}$ is the width of the distribution of $V(\mathbf{r})$. $D(r)$ is plotted in Fig. 2 for $x = 0.05$ and $p = 0.3$ for various numbers of MC steps, which serve as a rough measure of annealing time. Defect diffusion strongly reduces $D(r)$ and thus ΔV. The inset in Fig. 2 shows a blowup of $D(r)$ for the approximately equilibrated state. The initial reduction of $D(r)$ to about 10% of $D(0)$ on the scale of the nearest-neighbor separation of about 4.00Å(heavy bar) is due to the screening of the compensated 70% of Mn impurities by antisites, leaving only 30% active. Since $D(r)$ contains the potential squared, this leads to a reduction to about 9% (yellow region in the inset). The remaining contribution from uncompensated Mn (light blue region) decays on the typical length scale of 14.4Åassociated with their density, which is 0.3×0.05 per cation site. Clearly, ionic screening, *i.e.*, screening by the defects, is nearly perfect at 250°C. While the reduction of ΔV is thus substantial, we find that ΔV is still *not* small compared to the Fermi energy [1].

3. Valence-band holes

In this section we consider the properties of valence-band holes [6] in the impurity potential $V(\mathbf{r})$ due to the charged defects. In particular, we are interested in their spectrum and localisation properties. We employ the envelope function and parabolic-band approximations for the holes and start from the Hamiltonian $H = -\sum_i (\hbar^2/2m^*)\nabla_i^2 + V(\mathbf{r}_i)$. For material-specific calculations the detailed band structure should be taken into account, *e.g.*, using the 6-band Kohn-Luttinger Hamiltonian [7]. This should not change the qualitative results but is known to increase the mean-field T_c [7]. The hole Hamiltonian is written in a plane-wave basis and diagonalized numerically [1]. The calculations are done for spin-less holes, since the additional disorder introduced by the exchange interaction is found to be much smaller

than ΔV. We obtain the energy spectrum and normalized eigenfunctions $\psi_n(\mathbf{r})$. From the latter we calculate the inverse participation ratios

$$\mathrm{IPR}(n) = 1/\sum_{\mathbf{r}} |\psi_n(\mathbf{r})|^4 \tag{3}$$

of the states. The main physical content of the IPR is that it scales with system size for extended states but essentially remains constant for localized states. The IPR thus allows to estimate the position of the mobility edge in the valence band.

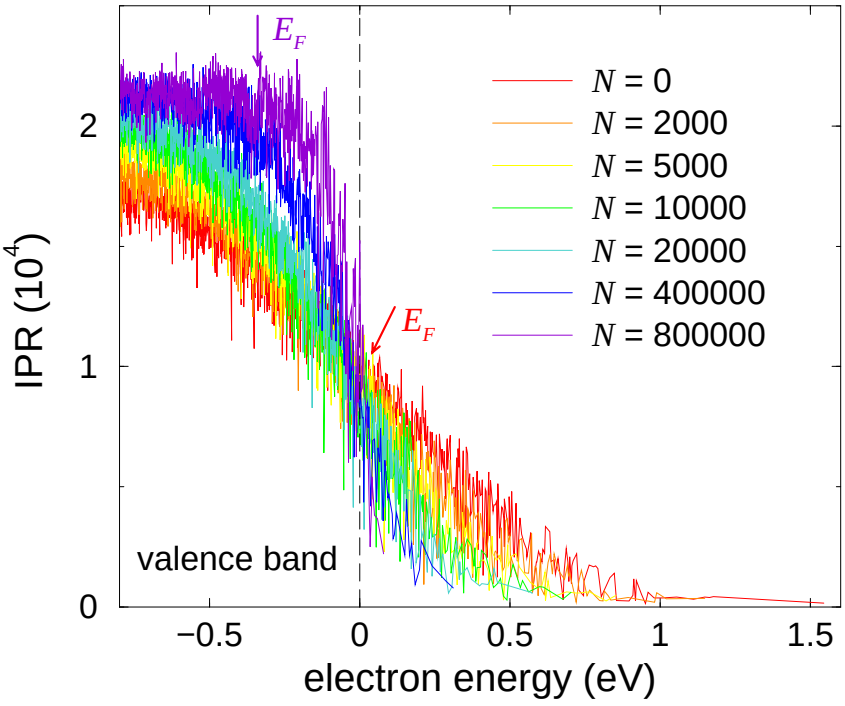


Figure 3. IPR as a function of electron energy for $x = 0.05$ and $p = 0.3$ after various numbers of MC steps increasing from the red to the violet curve. The Fermi energies for the random and the equilibrated case are also shown.

Figure 3 shows the IPR as a function of electron energy for the same parameters as above, $x = 0.05$ and $p = 0.3$, after various numbers of MC steps. The plot shows that uncorrelated defects would lead to the filling-in of the band gap by disorder, which is in contradiction to experiments. Thus correlated defects are required to explain the persistence of the energy gap. We have also studied the IPR for various system sizes and find that states in the flat region and the upper part of the slope are extended, whereas states in the band tail are localized, as expected. Figure 3 shows that the states at the Fermi energy become more and more extended with annealing, since the disorder potential decreases.

In Fig. 4 the IPR for fully annealed configurations is plotted as a function of Mn concentration x. The number of holes per Mn, p, has been chosen in accordance with experiments [3]. The change in the IPR-curves with x is rather weak due to the strong ionic screening. The main effect is the shift of the Fermi energy due to the varying hole density, which drives the Fermi edge into localized states below about 1% Mn. This qualitatively explains the metal-insulator transition observed in (Ga,Mn)As [3].

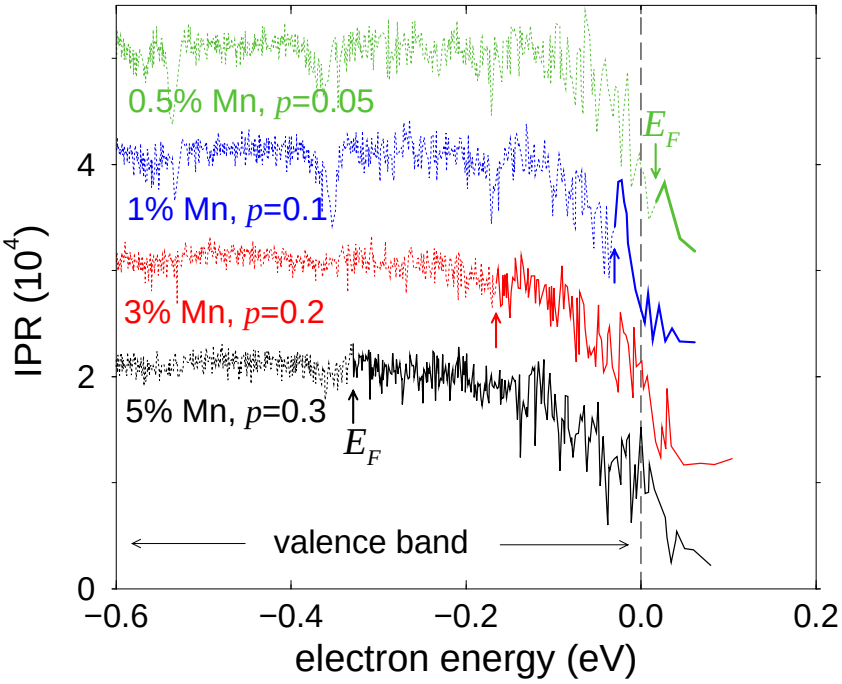


Figure 4. IPR as a function of energy for equilibrated configurations as a function of Mn concentration x with the number of holes per Mn, p, chosen in accordance with experiments [3]. The Fermi energies are also indicated.

4. Ferromagnetism

Finally, we turn to the magnetic properties. The bulk magnetisation is composed of contributions of the local Mn spins and of the holes. Since the exchange interaction between valence-band holes and local Mn spins is antiferromagnetic, these contributions are oriented oppositely. However, the hole contribution turns out to be very small. We study the magnetisation within a selfconsitent mean-field approximation, which we briefly outline in the following.

The starting point is the Hamiltonian of the coupled valence-band holes and Mn spins,

$$H = \sum_{n\sigma} \xi_n c^\dagger_{n\sigma} c_{n\sigma} - J_{\rm pd} \sum_i \mathbf{s}_i \cdot \mathbf{S}_i, \tag{4}$$

where $\mathbf{S}_i$ are Mn spins ($S = 5/2$) and

$$\mathbf{s}_i \equiv \sum_{n\sigma n'\sigma'} c^\dagger_{n\sigma} \psi^*_n(\mathbf{R}_i) \frac{\sigma_{\sigma\sigma'}}{2} \psi_{n'}(\mathbf{R}_i) c_{n'\sigma'} \tag{5}$$

are hole spin polarisations at the Mn sites. ξ_n and ψ_n are the hole eigenenergies and eigenfunctions, respectively, for vanishing magnetic interaction, $J_{\rm pd} = 0$. These have been obtained in the previous section—note that H contains the full Coulomb disorder potential. ξ_n includes the hole chemical potential.

We rewrite Eq. (4) as

$$H = \sum_{n\sigma} \xi_n c^\dagger_{n\sigma} c_{n\sigma} - \frac{J_{\rm pd}}{4} \sum_i \left[(\mathbf{s}_i + \mathbf{S}_i)^2 - (\mathbf{s}_i - \mathbf{S}_i)^2 \right] \tag{6}$$

and employ the imaginary-time functional integral. The two spin-squared terms are decoupled using Hubbard-Stratonovich transformations with auxilliary fields $\mathbf{h}^\pm_i$ coupling to $\mathbf{s}_i \pm \mathbf{S}_i$. The

auxilliary fields are then transformed to new fields $\mathbf{h}_i \equiv \mathbf{h}_i^+ + i\mathbf{h}_i^-$, $\mathbf{h}'_i \equiv \mathbf{h}_i^+ - i\mathbf{h}_i^-$. This leads to the Lagrangian

$$L = \sum_{n\sigma} c^*_{n\sigma}(\partial_\tau + \xi_n)c_{n\sigma} + iS\sum_i \dot{\phi}_i \cos\theta_i + \sum_i \frac{\mathbf{h}_i \cdot \mathbf{h}'_i}{J_{\rm pd}} - \sum_i (\mathbf{h}_i \cdot \mathbf{s}_i + \mathbf{h}'_i \cdot \mathbf{S}_i). \quad (7)$$

To obtain the mean-field theory we employ a saddle-point approximation. We assume $\mathbf{h}_i$ and $\mathbf{h}'_i$ to be constant in time but *not* in space, since we wish to retain the disorder effects. The holes and Mn spins are then easily integrated out. For the Mn spins this is best done in the Hamiltonian formalism. This leads to the grand potential

$$\beta\Omega_0 = -\,{\rm Tr}\ln\beta G^{-1}(i\omega) - \sum_i \ln\frac{\sinh[\beta h'_i(S+1/2)]}{\sinh(\beta h'_i/2)} + \frac{\beta}{J_{\rm pd}}\sum_i \mathbf{h}_i \cdot \mathbf{h}'_i \quad (8)$$

with the mean-field hole Green function

$$G^{-1}_{n\sigma n'\sigma'}(i\omega) = (-i\omega + \xi_n)\,\delta_{nn'}\delta_{\sigma\sigma'} - \sum_i \psi^*_n(\mathbf{R}_i)\,\frac{\sigma_{\sigma\sigma'}}{2}\cdot\mathbf{h}_i\,\psi_{n'}(\mathbf{R}_i). \quad (9)$$

The saddle-point equations are obtained by setting the derivatives of $\beta\Omega_0$ with respect to $\mathbf{h}_i$ and $\mathbf{h}'_i$ to zero,

$$\mathbf{h}_i = J_{\rm pd}\mathbf{M}_i = J_{\rm pd}\frac{\mathbf{h}'_i}{h'_i}SB_S(\beta Sh'_i), \quad (10)$$

$$\mathbf{h}'_i = J_{\rm pd}\mathbf{m}_i = -\frac{J_{\rm pd}}{\beta}\sum_{i\omega}\sum_{n\sigma n'\sigma'} G_{n\sigma n'\sigma'}(i\omega)\,\psi^*_{n'}(\mathbf{R}_i)\,\frac{\sigma_{\sigma'\sigma}}{2}\psi_n(\mathbf{R}_i) \quad (11)$$

with the usual Brillouin function $B_S(x)$. To actually evaluate Eq. (11) we diagonalize the hole sector of the Hamiltonian or, equivalently, the inverse Green function G^{-1}, writing $G^{-1} = \mathscr{O} g^{-1}\mathscr{O}^\dagger$, where $g^{-1}_{n\sigma} = -i\omega + \tilde{\xi}_{n\sigma}$ is diagonal. We assume the the mean-field Mn spin polarisation $\mathbf{M}_i$ to be collinear and choose the z axis along $\mathbf{M}_i$. Then G^{-1} is symmetric and $\mathscr{O}$ is orthogonal. Also, G^{-1} is then already diagonal in spin space so that we can diagonalize separately in each spin sector. We denote the components of $\mathscr{O}$ for spin sector σ by $\mathscr{O}_{nn';\sigma}$. The inversion of G is now trivial, $G = \mathscr{O} g \mathscr{O}^\dagger$. The frequency sum can finally be performed, since $\mathscr{O}$ does not depend on frequency. Introducing the new eigenfunctions

$$\tilde{\psi}_{n\sigma}(\mathbf{R}_i) = \sum_{n'} \psi_{n'}(\mathbf{R}_i)\,\mathscr{O}_{n'n;\sigma}, \quad (12)$$

Equation (11) then obtains the form

$$\mathbf{h}'_i = J_{\rm pd}\sum_{n\sigma} n_F(\tilde{\xi}_{n\sigma})\,\tilde{\psi}^*_{n\sigma}(\mathbf{R}_i)\,\frac{\sigma_{\sigma\sigma}}{2}\,\tilde{\psi}_{n\sigma}(\mathbf{R}_i). \quad (13)$$

The mean-field solution is obtained by iterating Eqs. (10) and (13).

Figure 5 shows the magnetisation curves for Mn and hole spins, again for $x = 0.05$ and $p = 0.3$ for random and equilibrium configurations. The hole-spin contribution to the total magnetisation is found to be very small. The shape of the Mn magnetisation curve becomes more "normal" and concave from below with annealing [1], except for a tail at higher temperatures, in good agreement with experimental annealing studies [2]. The anomalous shape for random defects is due to the localisation tendency of the holes, which leads to a shorter-range effective Mn spin interaction. This, together with the random positions of spins, leads to a broad distribution of effective fields acting on these spins. For higher temperatures, only a few spins with strong interactions carry most of the magnetisation, leading to the drawn out tail for random defects. The noise apparent on the curves is due to there being several

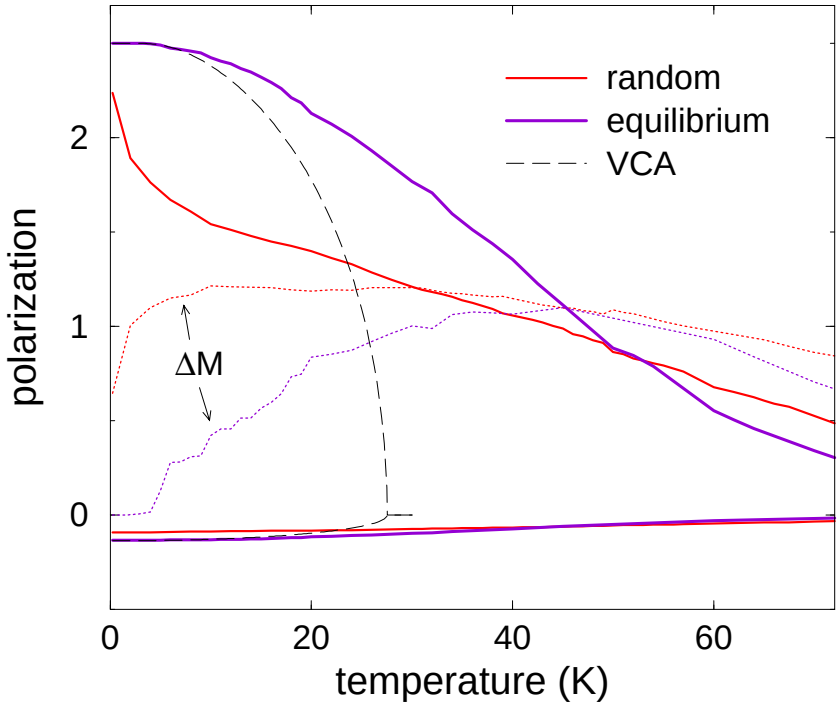


Figure 5. Magnetisation of Mn spins (up) and hole spins (down) as functions of temperature for $x = 0.05$ and $p = 0.3$ for random, partially annealed, and equilibrated configurations. The dotted curves give the standard deviations ΔM of Mn spins. For comparison, the long-dashed curves show the magnetisations obtained from a theory that totally neglects disorder.

saddle-points with similar free energy and total magnetisation. We also plot the standard deviations ΔM of the Mn spin polarisations. The standard deviation becomes comparable with the average Mn spin polarisation at intermediate temperatures below the Curie temperature T_c. This shows that the reduction of the total magnetisation with increasing temperature is initially dominated by disordering of large local moments. Only at higher temperatures the local moments also decrease.

The Curie temperatures are significantly larger than what one obtains from a virtual crystal approximation (VCA), neglecting disorder completely, see Fig. 5. It is an important open question whether this is an artifact of mean-field theory or indeed a physical result. However, the tails of the magnetisation curves with small average Mn spin polarisation but large standard deviation are dominated by a few anomalously strongly coupled spins. These are overemphasized by mean-field theory (remember that mean-field theory gives an incorrect finite polarisation even for two coupled spins). Thermal fluctuations should be effective in destroying the long-range order in this case, thus reducing T_c.

Finally, Fig. 6 shows magnetisation curves for equilibrated configurations at various Mn concentrations with the number of holes chosen as above. We see that the curves for smaller Mn and hole concentrations become more similar to the random limit in Fig. 5, which is easily understood since the holes become more localized.

5. Conclusions

We have shown that strong Coulomb interactions in highly compensated diluted ferromagnetic semiconductors naturally lead to strong correlations in the positions of charged defects. We also found that these correlations are essential for the description of transport properties, in

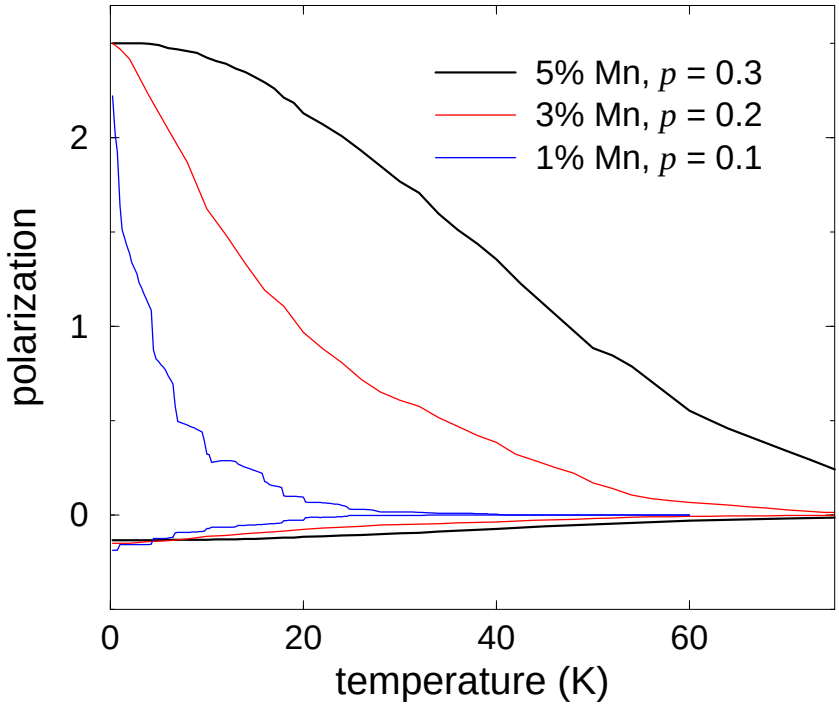


Figure 6. Magnetisation of Mn spins (up) and hole spins (down) as functions of temperature for various Mn and hole concentrations.

particular the metal-insulator transition, the persistence of the energy gap, and the shape of the magnetisation curves. It is a pleasure to acknowledge discussions with P. J. Jensen, J. König, U. Krey, W. Nolting, M. E. Raikh, F. Schäfer, and J. Schliemann.

References

[1] C. Timm, F. Schäfer, and F. von Oppen, Phys. Rev. Lett. (to be published), cond-mat/0201411.
[2] S. J. Potashnik, K. C. Ku, S. H. Chun, J. J. Berry, N. Samarth, and P. Schiffer, Appl. Phys. Lett. **79**, 1495 (2001); see also R. C. Lutz, P. Specht, R. Zhao, O. H. Lam, F. Börner, J. Gebauer, R. Krause-Rehberg, and E. R. Weber, Physica B **273–274**, 722 (1999).
[3] H. Ohno, Science **281**, 951 (1998); J. Magn. Magn. Mat. **200**, 110 (1999); H. Ohno and F. Matsukura, Solid State Commun. **117**, 179 (2001).
[4] B. I. Shklovskii and A. L. Efros, *Electronic Properties of Doped Semiconductors*, Solid-State Sciences **45** (Springer, Berlin, 1984).
[5] L. V. Keldysh and G. P. Proshko, Fiz. Tverd. Tela **5**, 3378 (1963) [Sov. Phys.—Solid State **6**, 1093 (1964–1965)].
[6] C. Timm, F. Schäfer, and F. von Oppen, submitted to Phys. Rev. Lett. (comment), cond-mat/0111504.
[7] J.M. Luttinger und W. Kohn, Phys. Rev. **97**, 869 (1955); M. Abolfath, T. Jungwirth, J. Brum, and A. H. MacDonald, Phys. Rev. B **63**, 054418 (2001); T. Dietl, H. Ohno, and F. Matsukura, Phys. Rev. B **63**, 195205 (2001).